 MCB, vol.5, no.3, pp.183-196, 2008

Role of Tissue Structure on Ventricular Wall Mechanics

Benjamin A. Coppola* **and Jeffrey H. Omens***,†

Abstract: It is well known that systolic wall thickening in the inner half of the left ventricular (LV) wall is of greater magnitude than predicted by myofiber contraction alone. Previous studies have related the deformation of the LV wall to the orientation of the laminar architecture. Using this method, wall thickening can be interpreted as the sum of contributions due to extension, thickening, and shearing of the laminar sheets. We hypothesized that the thickening mechanics of the ventricular wall are determined by the structural organization of the underlying tissue, and may not be influenced by factors such as loading and activation sequence. To test this hypothesis, we calculated finite strains from biplane cineradiography of transmural markers implanted in apical (n = 22) and basal (n = 12) regions of the canine anterior LV free wall. Strains were referred to three-dimensional laminar microstructural axes measured by histology. The results indicate that sheet angle is of opposite sign in the apical and basal regions, but absolute value differs only in the subepicardium. During systole, shearing and extension of the laminae contribute the most to wall thickening, accounting for $>90\%$ (transmural average) at both apex and base. These two types of deformation are also most prominent during diastolic inflation. Increasing afterload has no effect on the pattern of systolic wall thickening, nor does reversing transmural activation sequence. The pattern of wall thickening appears to be a function of the orientation of the laminar sheets, which vary regionally and transmurally. Thus, acute interventions do not appear to alter the contributions of the laminae to wall thickening, providing further evidence that the structural architecture of the ventricular wall is the dominant factor for its regional mechanical function.

1 Introduction

Systolic wall thickening in the left ventricle has long been considered an important functional measure because of its significant contribution to stroke volume (1, 2) and its sensitivity to local changes in perfusion (3) and metabolism (4). The observed amount and pattern of wall thickening cannot be explained by cell thickening alone; fiber shortening is similar across the wall in dog (5, 6), sheep (7), and human (8, 9), yet the radial thickening increases significantly from epicardium to endocardium in these and other studies (10, 11). In addition, the magnetic resonance imaging (MRI) studies of Rademakers et al. showed that wall thickening is correlated with crossfiber rather than fiber shortening, and attributed this to tissue tethering between the endocardium and epicardium (9). This suggests either a change in individual fibers during contraction, toward a more oval cross-section, or a rearrangement of a bundle of fibers as the wall thickens. There are a larger number of fibers across the wall during diastole than during systole (12), providing some evidence for the existence and function of fiber bundles. Additionally, there is transverse shear in the endocardium of sufficient magnitude and correct sign to account for endocardial wall thickening, and these shearing planes are closely aligned with the myocardial laminae (13).

Examination of the macrostructure of the heart reveals cleavage planes in the circumferential-radial and longitudinal-radial planes (12). Electron microscopy further reveals that these cleavage planes arise from the organization of my-

* Departments of Bioengineering, University of California, San Diego, La Jolla, CA 92093.

† Corresponding author. Departments of Medicine, University of California, San Diego, La Jolla, CA 92093. jomens@ucsd.edu; 9500 Gilman Dr. Mail Code 0613J, La Jolla, California 92093.

ofibers into laminar sheets, approximately 4 to 8 cells thick (13). These laminae exhibit variation in transmural and regional orientation (13). Slippage between laminae may result in transverse shearing and thus provide a mechanism for additional wall thickening. Costa and co-workers (14) explored this hypothesis by expressing wall thickening as the sum of the thickening due to each of three types of sheet motion: extension, thickening, and shearing. Using this same approach, Takayama et al. looked at the effect of changes in load during systole and diastole, and found the contributions to be qualitatively unchanged (15). There are changes in the deformation of the sheets during ventricular epicardial pacing relative to normal activation (5), but the relative contributions to wall thickening are unchanged.

In this study, we test the hypothesis that the thickening pattern of the ventricular wall occurs in a specific fashion based on the structural organization of the underlying tissue. To test this hypothesis, we implanted transmural bead arrays into the left ventricle of open-chest dogs and imaged them with biplane cineradiography. Finite strains were computed and referred to a histologically measured fiber-sheet coordinate system. We studied the contributions of sheet deformation to wall thickening during systole and diastole, with different loading conditions, and during ventricular pacing. We conclude that the contributions of the myocardial sheet deformations to ventricular wall thickening are a fixed property of the tissue that does not appear to fluctuate acutely. It appears as though the structural architecture of the ventricular wall is the dominant factor for its regional mechanical function.

2 Materials and Methods

All animal studies were performed according to the National Institutes of Health *Guide for the Care and Use of Laboratory Animals*. All protocols were approved by the Animal Subjects Committee of the University of California, San Diego, which is accredited by the American Association for Accreditation of Laboratory Animal Care.

The data described herein comes from four different sets of animal experiments performed in this laboratory (Table 1) assembled here to examine different experimental conditions. Three of these sets (groups A,B,C) have been previously published in some form (5, 15, 16); the raw data has been re-analyzed to fit the scope of this paper. The fourth set (group D) is original data with ventricular pacing. Several aspects of the experiments are identical, and will be discussed first.

2.1 Common Preparation

Adult mongrel dogs (19–27 kg, n = 22) were anesthetized with intravenous propofol (6 mg/kg), intubated, and mechanically ventilated with isoflurane (0.5–2.5%), nitrous oxide (2 l/min), and medical oxygen (2 l/min) to maintain a surgical plane of anesthesia. The heart was exposed via a median sternotomy and a left thoracotomy at the fourth intercostal space, and then placed in a pericardial cradle. An 8-Fr pigtail micromanometer catheter (Millar Instruments, Houston, TX) was inserted through a 9-Fr arterial introducer placed in the left femoral artery, and the catheter tip was advanced into the LV. LV pressure was monitored with the pigtail micromanometer catheter, and the pressure was matched with that recorded from the side holes of the same catheter that was connected to a fluid-filled transducer. Columns of four to six gold beads (0.8 mm diameter) were placed from the epicardial surface with the use of a trocar (14). The apical marker implantation site for the set of three columns was selected approximately one-third of the distance from apex to base along the LV long axis in the anterior wall. After marker implantation, larger (2.0 mm diameter) lead beads were sewn to the epicardial surface above each column, as well as at the apex of the LV (apex bead), and at the bifurcation of the left main coronary artery (base bead). These epicardial markers were used to define a local set of circumferential, longitudinal, and radial cardiac coordinate axes $\{X_1, X_2, X_3\}$ at each site, as previously described (17).

Each animal was positioned in a biplane radiography system, and synchronous biplane cineradiographic images (125 frames/s) of the bead markers were digitally acquired with mechanical ventilation suspended at end expiration. After the func-

Table 1: Description of Data Sources. The four sources (A-D) of the data in this paper. Groups A & B utilized only the control data from these experiments. The largest complete sets of data are end-systolic control data at the apex (n=22) and base (n=12).

Group	Source	Intervention	Site	Sample Size
A	Ashikaga et al. 2004 #1	Control only	Apex/Base	6
B	Ashikaga et al. 2004 #2	Control only	Apex	5
C	Takayama et al. 2002	Preload & Afterload	Apex/Base	6
D	Original data	Endo- and Epicardial Pacing	Apex	5

tional data acquisition was complete, the animals were euthanized with pentobarbital sodium and the heart arrested and perfusion fixed with 2.5% buffered gluteraldehyde at the end-diastolic pressure measured during the atrial paced run in the study, as described previously (18). The fixed, silastic-filled heart was skewered from the apical dimple to the mitral aspect of the aortic valve, to define the LV long axis (19). To avoid the distortional effects of dehydration and embedding, histological measurements were obtained using freshly fixed heart tissue (14, 18). In the transmural block of tissue within the implanted bead set, the mean fiber (α) and sheet angles (β) were determined from epicardium to endocardium using the methods of Costa (14) or Ashikaga (18).

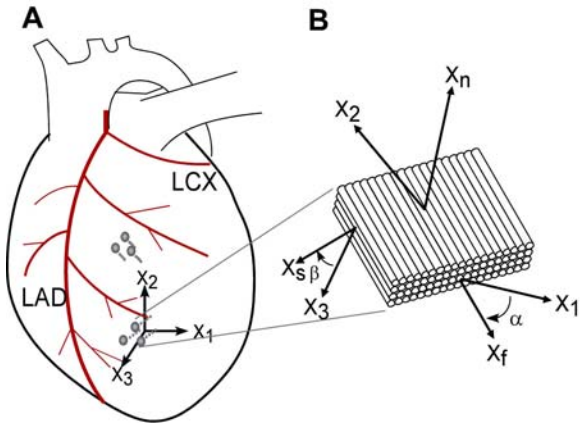

Figure 1: A: schematic representation of the left ventricle with bead arrays at the apex and base (1/3 and 2/3 of the distance from apex and base, respectively). X_1, circumferential axis; X_2, longitudinal axis; X_3, radial axis; LAD, left anterior descending; LCX, left circumflex. B: schematic representation of local fiber-sheet axes. Fiber angle (α) was measured in the $X_1 - X_2$ plane at each wall depth with reference to positive X_1. Sheet angle (β) was measured in the plane perpendicular to the fiber angle at each wall depth with reference to positive X_3. X_f, fiber axis, X_s, sheet axis, X_n, axis oriented normal to the sheet plane.

2.2 Differences between Preparations

In two sets of animals (groups A & C) a second set of three columns was implanted at the basal site, approximately two-thirds of the distance from the apex to the base. Fig. 1A depicts this arrangement. In addition, an implantable micromanometer (Konigsberg Instruments; Pasadena, CA) replaced the Millar catheter in these groups. In group C, a snare was placed around the inferior vena cava (IVC) for the preload studies. Group A differed the most - the chest was closed and the animal recovered for 7-10 days. Functional data was acquired with the animal lightly sedated and hanging in a sling as described in (16). We compared the mean sheet angles of Group A with Groups B-D and concluded that they were not significantly different. The relative contributions to wall thickening were also unchanged. As a result, we chose to combine the data sets.

2.3 Experimental Protocol

All animals (groups A-D) were included as control data for the analysis of end-systolic function. In total, there were 22 animals with apical bead arrays and 12 with basal bead arrays. All other experimental procedures involved only subsets of animals.

2.3.1 Preload (group C)

Apical (n=6) and basal (n=6) bead arrays. The preload studies are described in (15). In brief, dextran was rapidly infused into the heart to raise end-diastolic pressure (EDP) to ∼20 mmHg. The IVC was then abruptly occluded. Cineradiographic and hemodynamic data were acquired at levels of high EDP (17-22 mmHg), medium EDP (12-14 mmHg), low EDP (7-9 mmHg), and a reference state (3-4 mmHg).

2.3.2 Afterload (group C)

Apical (n=6) and basal (n=6) bead arrays. The afterload studies are also described in (15). Briefly, methoxamine (5 to 10 μg · kg-1 · min-1) was infused to elevate LV end-systolic pressure (ESP) by at least 35 mmHg. During methoxamine infusion, dextran was transfused as needed to elevate EDP or IVC occlusion as needed to reduce EDP was used to ensure that the EDP was matched with the initial value in each animal (within 1 mmHg). Biplane cineradiography and hemodynamic data were then recorded.

2.3.3 Pacing (group D)

Apical bead array only (n = 5). Atrial pacing was performed by stimulating LA electrodes, and LV pacing was performed by stimulating both LA and LV electrodes (LA-LV delay = 35 ms), via a square-wave constant-voltage electronic stimulator (model SD9; Grass Instruments, Quincy, MA) at a frequency 20% above baseline heart rate to suppress native sinus rhythm. Stimulation parameters (voltage 10% above threshold, duration 8 ms, and frequency) were kept constant in each animal. Each animal was positioned in a biplane radiography system, and synchronous biplane cineradiographic images (125 frames/sec) of the bead markers were digitally acquired with mechanical ventilation suspended at end expiration. Recordings were obtained during atrial pacing and then following approximately 2 to 5 minutes of endo- or epicardial pacing (to achieve a steady hemodynamic state). Atrial pacing was continued between ventricular pacing runs.

2.4 Finite strain analysis

The following methods were common to all animals. Biplane cineradiographic images (125 frames/s) from the X-ray image intensifiers were spherically corrected, and the 3-D coordinates of the bead markers were reconstructed in each frame based as described in Ashikaga et al. (18). A continuous polynomial position field that mapped the beads in the undeformed reference configuration to those in the deformed configuration was determined (18, 20). The order of the polynomial is at most linear in the circumferential and longitudinal directions, and the maximum order in radius is typically quadratic. With this continuous polynomial mapping from reference position to current position, differentiation with respect to reference position gives the deformation gradient tensor, $\mathbf{F}$, which depends on position. The Lagrangian Green's strain tensor was then calculated as $0.5(\mathbf{F}^T\mathbf{F} - \mathbf{I})$ at various values of reference wall depth, where $\mathbf{F}^T$ is the transpose of $\mathbf{F}$ and $\mathbf{I}$ is the identity matrix.

Six independent finite strains [circumferential (E_{11}), longitudinal (E_{22}), and radial (E_{33}) strains, circumferential-longitudinal shear (E_{12}), longitudinal-radial shear (E_{23}), and circumferential-radial sheer (E_{13})] were computed in the local cardiac coordinate system of circumferential, longitudinal, and radial axes (X_1, X_2, X_3), which were subsequently used to compute another set of six finite strains [fiber strain (E_{ff}), sheet strain (E_{ss}), strain normal to the sheet plane (E_{nn}), fiber-sheet shear (E_{fs}), sheet shear (E_{sn}), and fiber-normal shear (E_{fn})] in the local fiber-sheet coordinate system (X_f, X_s, X_n) through an orthogonal transformation to convert the strain tensor using the values of α and β at each depth (14). The local fiber-sheet coordinate system defines the myofiber axis (X_f), the sheet axis (X_s) that lies within the sheet plane and is perpendicular to X_f, and the orthogonal X_n axis oriented normal to the sheet plane, as shown in Fig. 1B.

Finite strains were calculated in fiber-sheet coordinates with local activation as the reference state. During atrial pacing, this coincided with the peak of the ECG R wave. In the case of ventricular pac-

ing, the time of local stimulus was used as the reference state. If an aortic flow probe was present, it was used to determine the time of end systole. Otherwise, the pressure at the nadir of the dicrotic notch of the central aortic pressure was used to estimate the time of end systole from the micromanometer tracing. Strains were determined at three wall depths: 20% (sub-epicardium), 50% (midwall), and 80% (sub-endocardium).

2.5 Contributions of fiber-sheet strains to wall thickening

Deformations expressed in the cardiac coordinate system can be related to the laminar architecture as described in (14). Because the sheet structure is believed to provide a mechanism for increased wall thickening, we can rewrite the radial strain in terms of contributions due to sheet motion, as in Eq. 1.

$$E_{33} = E_{ss}\cos^2\beta + E_{nn}\sin^2\beta + 2E_{sn}\sin\beta\cos\beta \quad (1)$$

The terms on the right-hand side of Eq. 1 can be interpreted as contributions due to sheet extension (=$E_{ss}\cos^2\beta$), sheet thickening (=$E_{nn}\sin^2\beta$), and sheet shearing (=$2E_{sn}\cos\beta\sin\beta$) during wall thickening. Illustrations are provided in Fig. 2. Conversely, during wall thinning they represent sheet shortening, thinning, and shearing of the opposite sense.

2.6 Statistical analysis

Values are means ± SD. Repeated measures analysis of variance (RMANOVA) was used whenever applicable (see RESULTS for details). Tukey's method was used for ANOVA post hoc analysis. Statistical tests were performed with SigmaStat 3.0 (SPSS, Chicago, IL). Statistical significance was accepted at $P < 0.05$.

3 Results

3.1 Sheet Angles

Fig. 3 shows sheet angle (β) as a function of transmural depth for the apical and basal measurement sites (n = 22 and n = 12, respectively).

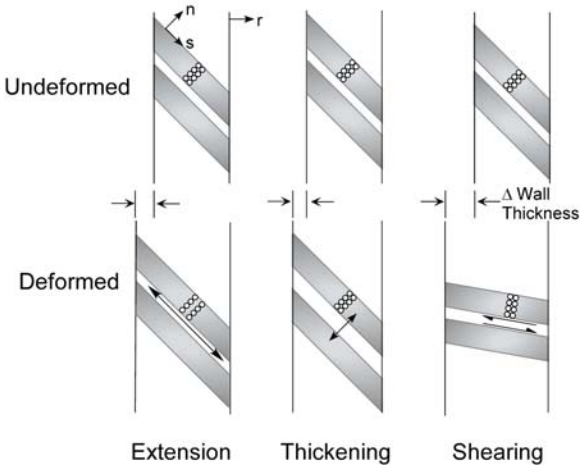

Figure 2: Contributions of different types of sheet deformation to wall thickening. Schematics show how a portion of the wall can thicken from an undeformed (top) to deformed (bottom) state, based on sheet movement. A: extension of the sheets, B: thickening of the sheets, C: shearing between sheets. Wall thickening is indicated by the widening of the vertical bars, i.e. an increase in the radial direction, r. Open circles represent myofibers, gray bars represent sheets. s, sheet direction; n, sheet normal direction.

As opposed to the linear transmural distribution of fiber angle, β was a nonlinear function of depth, with the largest absolute value occurring at the midwall (-32.2±17.7° and +25.9°±18.3 at apex and base, respectively). The sign of the sheet angle was negative at all depths at the apex, but only in the sub-epicardium at the base. There was a significant transmural gradient at both sites by one-way RMANOVA. Pairwise comparisons revealed a significant difference between midwall and sub-endocardial sheet angles at the apex, and between sub-epicardial and midwall sheet angles at the base. The interaction between depth and site could not be tested for significance due to unequal sample size. Instead, unpaired t-tests were used to compare the two sites at each depth. By this analysis, the sheet angle at the apex was significantly different from the base at each depth. In the subset of animals that included both apical and basal data (groups A and C), a two-way

RMANOVA was performed with depth and region as repeated variables. With this smaller sample size (n = 12), the apex was significantly different from the base but the transmural gradient became insignificant. There was also an effect of region on transmural gradient.

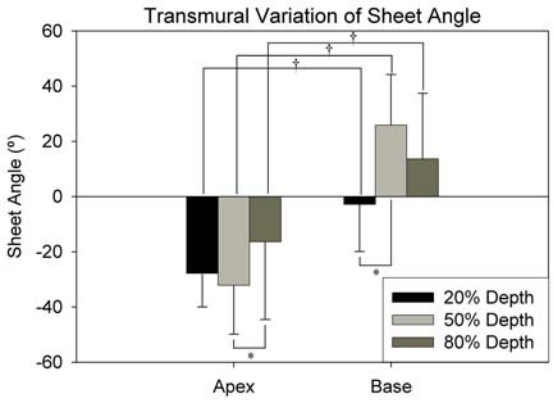

Figure 3: Sheet angles. Angle = 0° indicates a radial orientation. Sheet angle has opposite sign at apical and basal sites, but similar absolute values. The largest angle occurred at the midwall of each site. There was a significant transmural gradient at each site (RMANOVA, $p<0.05$). * $p < 0.05$ vs other depths. At each depth, the base was significantly different from the apex. † $p < 0.05$ vs. same depth, by unpaired t-test.

3.2 End-Systolic Contributions to Wall Thickening

Transmural deformation of the ventricular wall can be expressed in terms of the laminar architecture as described by Eq. 1 (see METHODS). Fig. 4 shows how these three terms contribute (as a percentage) to the overall wall thickening at end systole. At the apex (n=22), sheet extension and shearing were the dominating components, contributing 47.2 and 46.6% as a transmural average. There was no significant transmural gradient. At the base (n=12), sheet extension and shearing were also dominant, but in addition there was a significant transmural gradient. Pairwise comparisons showed a decrease in sheet shearing and an increase in sheet extension in the sub-epicardium. This shift from shear to extension in part reflects the more radial orientation of sheets in the basal sub-epicardium. Unpaired t-tests showed differences in each component of wall thickening between apex and base in the sub-epicardium only. Additionally, in the subset of animals that included both apical and basal data (groups A and C), a two-way RMANOVA was performed with depth and region as repeated variables. This also showed a significant effect of both depth and region, with no significant interaction between the two. These results were not qualitatively different from those presented in Fig. 4.

3.3 Interventions

The magnitude of wall thickening can be altered by external factors. Therefore, it is possible that such interventions would also affect the relative contributions to wall thickening. For example, a decrease in afterload increases the magnitude of wall thickening. This increase might be accompanied by an increase in shearing of sheets that is greater than the increase of the other components of wall thickening, thus changing the relative proportions. To test this, we examined the effects of diastolic and systolic load, as well as activation sequence.

3.3.1 Diastolic Wall Thinning

In a subset of animals (group C) we examined the contributions to wall thinning during diastolic inflation as a function of load. Fig. 5 illustrates each component of wall thickening when inflating hearts from a reference configuration of 3 mmHg to a deformed configuration of 8 mmHg (“Low”), 13 mmHg (“Medium”), or 18 mmHg (“High”). Error bars tend to be bigger at lower loads due to smaller deformation and therefore greater relative noise levels. A three-way RMANOVA (depth, pressure, site) showed only significant differences with depth. None of the components of wall thickening were significantly altered by diastolic load, at either the apex or base. Similarly, the transmural gradients were not significantly altered by load. There were significant transmural gradients in sheet extension and shearing at medium and high loads (by one-way RMANOVA).

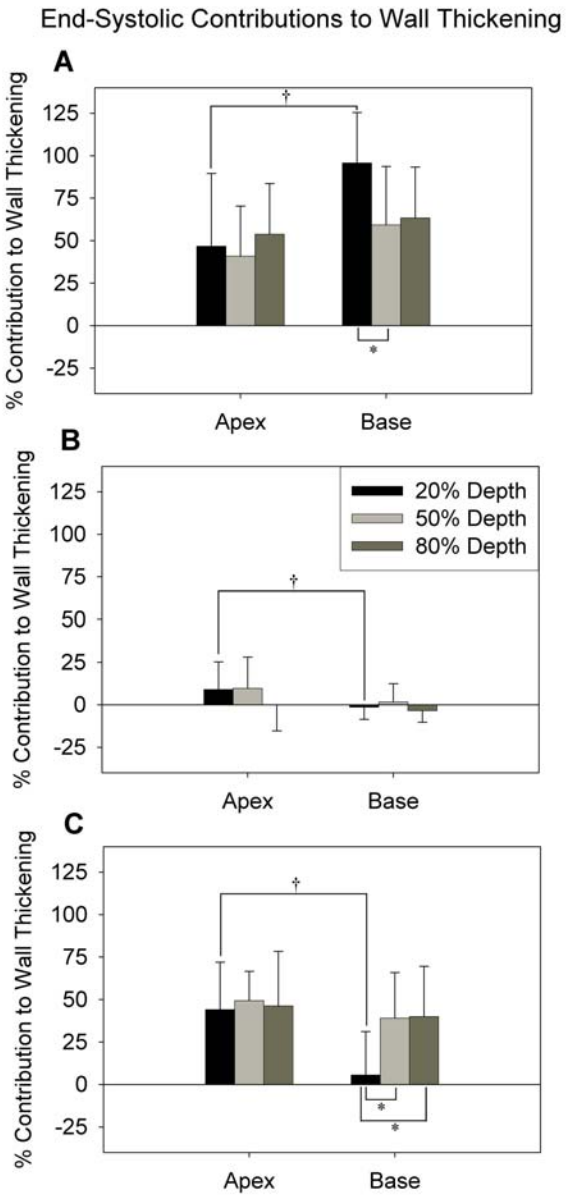

Figure 4: End-systolic contributions to wall thickening. Contributions to wall thickening due to sheet extension (A), sheet thickening (B), and sheet shearing (C). Relative contributions of sheet deformation to wall thickening were similar at both sites. There were significant transmural gradients due to sheet extension and sheet shearing at the basal site (RMANOVA, $p<0.05$). * $p < 0.05$ vs other depths. At the sub-epicardium only, the relative contributions to wall thickening were significantly different between the apical and basal sites († $p < 0.05$ vs. same depth, by unpaired t-test).

We also compared the contributions to wall thickening vs. wall thinning (i.e. systolic versus diastolic contributions). The contributions of sheet extension and shearing were significantly different between systole and diastole at the apical site, but not at the basal site. The type of deformation did not affect the transmural gradient at either site (two-way RMANOVA).

3.3.2 *Effect of Afterload on Contributions to Wall Thickening*

In the same subset of animals (group C), we examined the effect of load on the contributions to systolic wall thickening. Fig. 6 shows the changes in each component when peak systolic pressure was raised from 119 $\pm$ 22 to 169 $\pm$ 23 mmHg without significant change in end-diastolic pressure. Sub-epicardial values were excluded because the increased afterload reduced the magnitude of the strains; in some animals this magnitude became less than the uncertainty of the measurement. There were no significant differences in any of the components at the midwall or subendocardial levels at either the apex or base (two-way RMANOVA).

3.3.3 *Effect of Activation Sequence on Contributions to Wall Thickening*

In a different subset of animals (Group D), we investigated the effect of activation sequence on the contribution to wall thickening. Fig. 7 shows the time course of wall thickening over a single cardiac cycle in a representative animal (depth = 50%), beginning at local depolarization. Stacked bars indicate contributions of sheet motion to overall wall thickening (bar height = E_{33}). Fig. 7A shows an atrial paced beat with normal ventricular activation. Sheet thinning occurs during the isovolumic contraction, which acts to inhibit the normal wall thickening. During the ejection phase, all three components act together to increase wall thickening (extension = 12%; thickening = 22%; shearing = 66% at peak wall thickening). Their relative contributions were fairly constant, with sheet thickening becoming somewhat more important approaching peak wall thickening. The isovolumic relaxation phase varied much

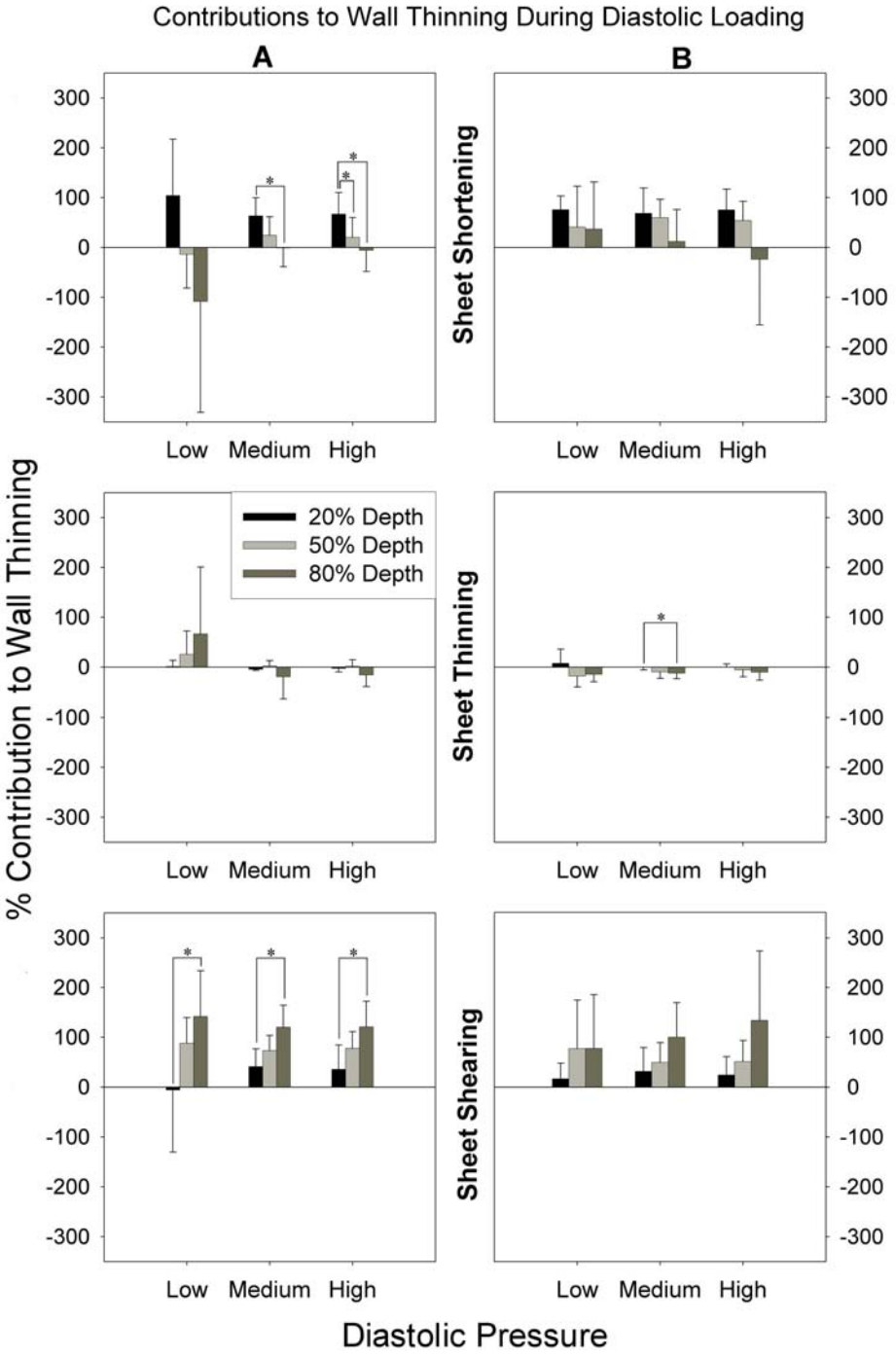

Figure 5: Contributions of sheet deformation to wall thinning during diastolic loading. Bars show relative contributions during diastolic inflation from a reference configuration of 3 mmHg to a deformed configuration of 8 mmHg ("Low"), 13 mmHg ("Medium"), or 18 mmHg ("High"). Contributions due to sheet shortening, thinning, and shearing were similar at apex (A) and base (B), and their transmural gradients were not significantly affected by diastolic load (* $p < 0.05$ vs. other depths).

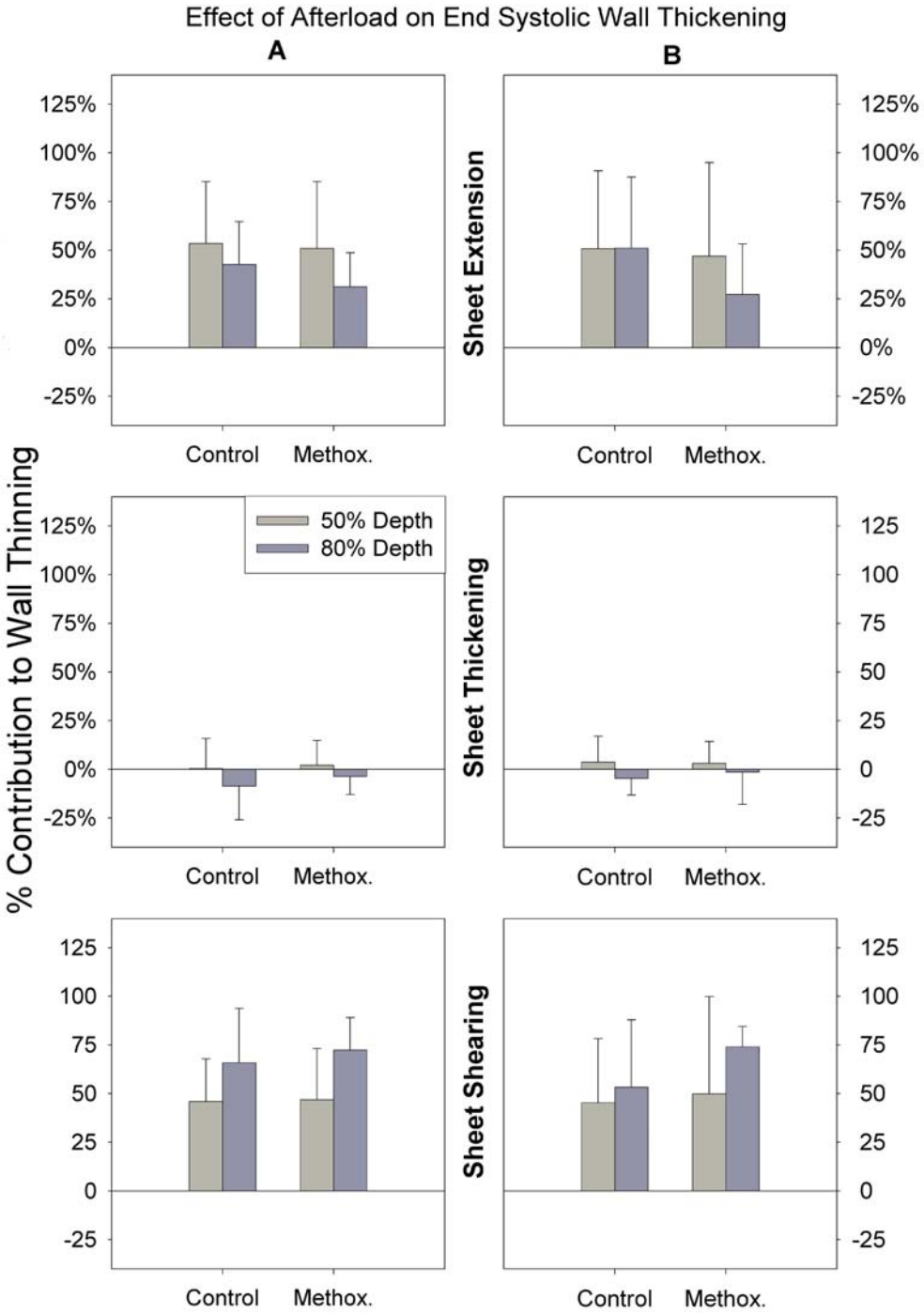

Figure 6: Effect of afterload on wall thickening. Bars indicate relative contributions to wall thickening at midwall and sub-endocardial depths. Increased afterload was achieved by administering methoxamine ("Methox."). There were no significant differences at the apex (A) or base (B) in any of the contributers. Sub-epicardial values were excluded due to insufficient strain magnitude to perform calculation.

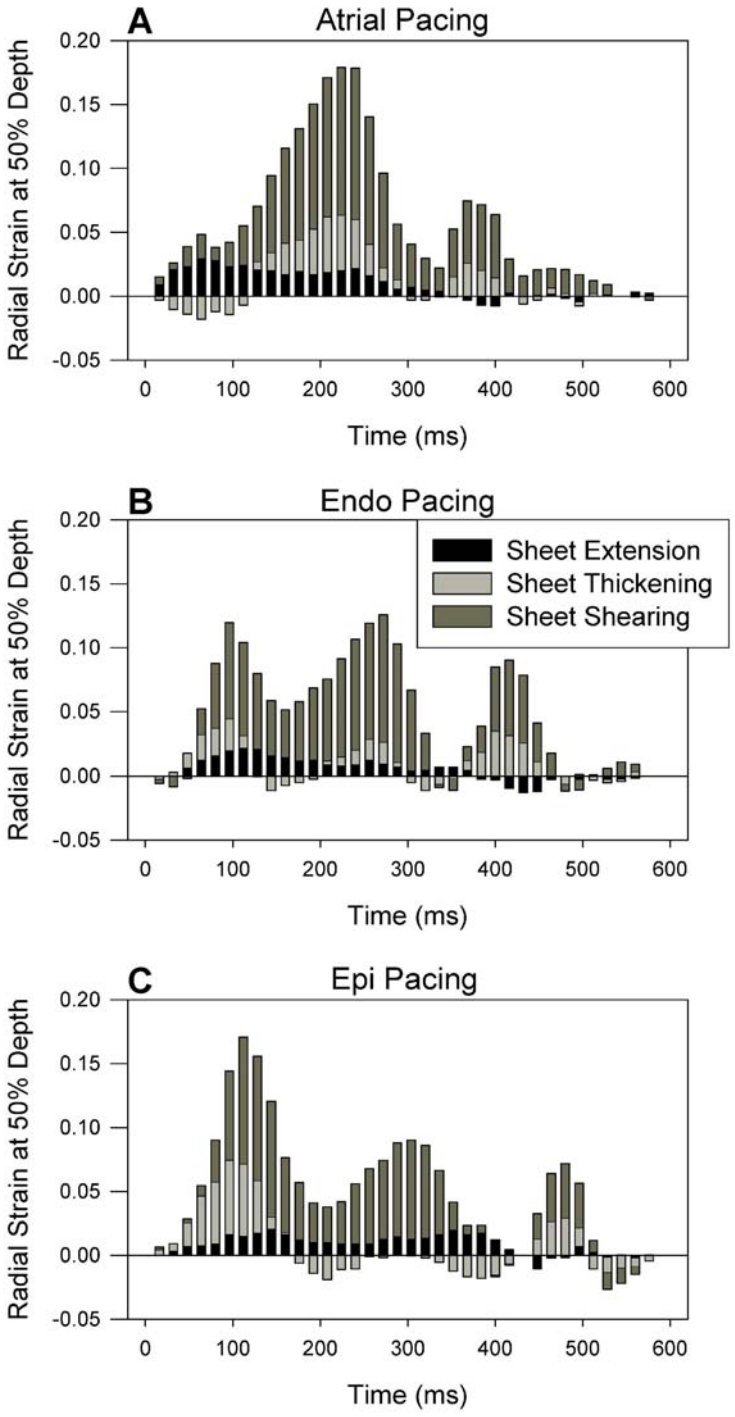

Figure 7: Time course of wall thickening during pacing during atrial pacing (A), local endocardial pacing (B), or local epicardial pacing (C). Bar height indicates magnitude of radial strain at 50% depth as a function of time for one cardiac cycle, in a representative animal. Stacked bars distinguish the relative contributions of the different sheet motions. Though the time courses are different, the contributions of sheet deformation to wall thickening are relatively constant throughout the cycle as well as with different pacing modes. Differences tended to be greatest during the isovolumic phases.

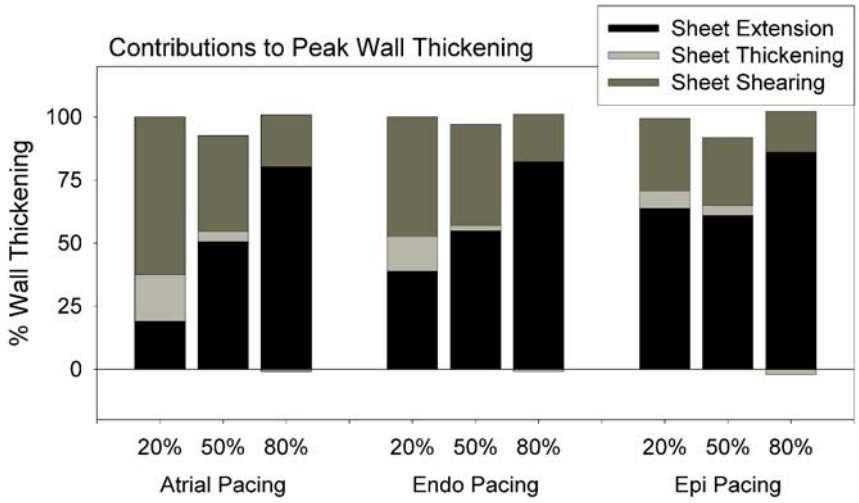

Figure 8: Average contributions to wall thickening during pacing. Stacked bars represent the average of each of the components of wall thickening at three transmural depths. For all components, there was a significant transmural gradient; however, ventricular pacing (endocardial or epicardial) was not significantly different from atrial pacing, nor was there a significant interaction with depth (2-way RMANOVA).

from animal to animal. In this example, it primarily consisted of sheet shearing. Fig. 7B and 7C depict the time course of wall thickening during local endocardial and epicardial pacing, respectively. Despite the differences in timing of peak wall thickening, the contributions to wall thickening was similar across pacing modes.

Fig. 8 shows the average value of each component during each of the three pacing modes. Only the time of peak wall thickening is shown. There was a significant transmural gradient in all components, but not a significant effect of pacing or an interaction between pacing and depth according to a two-way RMANOVA.

4 Discussion

In this paper, we analyze the motion of myocardial sheets under a variety of circumstances, including passive inflation and active contraction with varying loads, as well as different ventricular activation sequences. The deformation measurements spanned the wall transmurally at apical and basal sites. The major findings of this study are that the mechanisms of wall thickening/thinning may be different in diastole than in systole at the apex, but are independent of load at either site. Additionally, despite significant differences in the sign of sheet angle at the apex and base, there were minimal differences in the relative contributions to wall thickening. Lastly, the sequence of activation did not alter the thickening mechanics when assessed at peak wall thickening.

4.1 Diastolic vs. Systolic Deformation of the Wall

For the first time we compared, quantitatively, the relative contributions to wall thickening during diastole and systole. There were significant differences in sheet extension and shearing between diastole and systole at the apical site, but not the basal site, when compared with a two-way RMANOVA. Takayama and co-workers (15) concluded that the contributions were qualitatively similar during diastole and systole. Our own quantitative analysis of the available raw data disagrees somewhat. We show a significant change at the apex, manifested as a shift from sheet shearing to extension. Nevertheless, sheet shearing remains the predominant mode of wall thickening, consistent with the fundamental conclusions of Takayama (15) and Costa (14). In addition, a comparison of Figs. 4 and 5 seems to show larger transmural gradients during diastole than systole. However, a two-way RMANOVA with strain type

(diastolic inflation to 18 mmHg vs. end-systolic) and depth found that there was no significant interaction of strain type on transmural gradient in any component. Therefore, this appears to be an artifact due to the difference in sample size between the two sets.

4.2 Choice of mean sheet angles

In this analysis, we chose to use the mean sheet angle for our calculations. This has previously been used when making histological measurements (14, 18, 21, 22) or using diffusion tensor MRI (DTMRI) (23-25). This is also the typical approach to quantifying the fiber angle, which varies linearly from epicardium to endocardium (19) and has a narrow dispersion (angular SD $<$ 20°) (26). However, the structural arrangement of the laminae is somewhat more complex. Our own unpublished observations indicate that there can be larger dispersions in the sheet angle, particularly nearing the endocardium. In addition, the sheet angle can have a bimodal distribution, again near the endocardium. This has been described in Hooks et al. (21), in which the authors observed a "dominant lamina population with interspersed small 'pockets' of laminae approximately perpendicular to the principal alignment." The effects of both dispersion and bimodal populations on myocardial material properties is unknown, and may very well play an important role in the function of the myocardium, especially wall thickening. Thus, use of the average value of sheet angle may be inaccurate and therefore the results misleading. Further examination of the functional effects of the detailed laminar structure is ongoing in this laboratory.

4.3 Differences among species

In addition to dog, sheet angles have been measured in mice (27), rat (25), sheep (22), pig (28), and human (29). Mice have the most similar pattern of sheet angle to the dog, remaining approximately constant near –40° from epicardium to endocardium (27). Rat sheets are orientated more radially than dogs in the outer half; in the inner half, the orientation differed in sign, i.e. they are negative at the base and positive at the apex (25). Sheep sheets follow a notched pattern when examined in a lateral wall site; sheets are oriented positive at the epicardium, negative in the midwall, and positive again at the endocardium (22). Studies in pig and human do not provide data in a form suitable for direct comparison. Interestingly, however, Dou et al. show with DTMRI that the contributions to wall thickening vary greatly based on circumferential location (29). Their anterior wall measurements are consistent with the data given here. It is not clear from their data whether or not these differences in contributions to wall thickening are correlated with differences in sheet orientation.

4.4 Activation sequence

The transmural sequence of activation could also play a role in wall thickening. Myofibers are physically coupled between the endocardium and the epicardium, such that the deformation of one depends on the deformation of the other. This is a concept known as tissue tethering (30) (5). Because the epicardial and endocardial fiber angles are roughly perpendicular, endocardial fiber shortening will result in epicardial cross-fiber shortening and vice-versa. In the normal sequence of activation (endo -> epi), the earlier activation of the endocardium causes epicardial deformation of the sheets that results in a unique profile of contributions to wall thickening. When the activation sequence is reversed, the epicardium now deforms as a result of its own fiber shortening, and causes an endocardial deformation. This theory may have merit due to the early differences between endocardial and epicardial pacing (Fig. 7). However, the effect appears to be small, as the relative contributions at peak wall thickening are not significantly different.

4.5 Limitations

There is a possibility that the insertion of beads into the myocardium causes significant damage, particularly in the short term. Due to surgical trauma and loss of the normal intra-thoracic pressure gradient, wall thickening is reduced in open-chest preparations. If the chest is closed and the animal is allowed to recover, the magnitude of

wall thickening increases while leaving the relative contributions to wall thickening unchanged (7). This suggests that neither bead insertion injury nor the open-chest nature of the experiments has any qualitative effect on the results. DTMRI of a beating heart (29) is an alternative method that can provide non-invasive measurements throughout the whole heart, but with limited resolution.

There are also limitations related to the histological assessment of sheet angle. The methods were somewhat different for the estimation of mean angle in groups A and B compared to groups C and D. In groups A and B, cleavage plane angles were measured in circumferential-radial and longitudinal-radial sections. The sheet angles were then reconstructed from the two views using a least squares fitting routine to provide a transmural distribution. For groups C and D, sheet angle was measured directly in a plane perpendicular to the local fiber direction. These measurements were performed from epicardium to endocardium at approximately 1mm intervals. The sheet angles used in the analysis were then interpolated at 20, 50, and 80% depth (linear interpolation using two nearest neighbors).

In conclusion, the myocardial wall deforms radially in a similar pattern with respect to the underlying sheet architecture regardless of whether it is thickening or thinning, at the apex or base, at different depths, different loads, or with different activation patterns. Myocardial sheets have a fixed behavior relative to wall motion that we were not able to change acutely. We do not rule out the possibility of chronic changes, which may provide a mechanism for wall thickening changes during disease states such as heart failure.

Acknowledgement: This work was supported by Medtronic Inc. and UC Discovery Grant ITL06-10159 and NIH- HL32583. The authors would like to thank Dr. James W. Covell for valuable discussions and ideas concerning this manuscript. We would also like to thank Aundrea Graves, Katrina Go, Henry Tse, Leonard Lee, Harn Chiu, and Katrina Go for technical and surgical assistance.

References

1. Dumesnil, J. G. & Shoucri, R. M. (1991) *J Appl Physiol* **70,** 48-54.

2. Gould, K. L., Kennedy, J. W., Frimer, M., Pollack, G. H. & Dodge, H. T. (1976) *The American Journal of Cardiology* **38,** 322-331.

3. Gallagher, K., Gerren, R., Stirling, M., Choy, M., Dysko, R., McManimon, S. & Dunham, W. (1986) *Circ Res* **58,** 570-583.

4. Perrone-Filardi, P., Bacharach, S., Dilsizian, V., Maurea, S., Frank, J. & Bonow, R. (1992) *Circulation* **86,** 1125-1137.

5. Ashikaga, H., Omens, J. H., Ingels, N. B., Jr. & Covell, J. W. (2004) *Am J Physiol Heart Circ Physiol* **286,** H2401-7.

6. Waldman, L. K., Nosan, D., Villarreal, F. & Covell, J. W. (1988) *Circ Res* **63,** 550-62.

7. Cheng, A., Langer, F., Rodriguez, F., Criscione, J. C., Daughters, G. T., Miller, D. C. & Ingels, N. B., Jr. (2005) *Am J Physiol Heart Circ Physiol* **289,** H1234-1241.

8. MacGowan, G. A., Shapiro, E. P., Azhari, H., Siu, C. O., Hees, P. S., Hutchins, G. M., Weiss, J. L. & Rademakers, F. E. (1997) *Circulation* **96,** 535-541.

9. Rademakers, F., Rogers, W., Guier, W., Hutchins, G., Siu, C., Weisfeldt, M., Weiss, J. & Shapiro, E. (1994) *Circulation* **89,** 1174-1182.

10. Sabbah, H. N., Marzilli, M. & Stein, P. D. (1981) *Am J Physiol Heart Circ Physiol* **240,** H920-926.

11. Gallagher, K. P., Osakada, G., Matsuzaki, M., Miller, M., Kemper, W. S. & Ross, J., Jr (1985) *Am J Physiol Heart Circ Physiol* **249,** H241-248.

12. Spotnitz, H. M., Spotnitz, W. D., Cottrell, T. S., Spiro, D. & Sonnenblick, E. H. (1974) *J Mol Cell Cardiol* **6,** 317-31.

13. LeGrice, I. J., Takayama, Y. & Covell, J. W. (1995) *Circ Res* **77,** 182-93.

14. Costa, K. D., Takayama, Y., McCulloch, A. D. & Covell, J. W. (1999) *Am J Physiol* **276,** H595-607.

15. Takayama, Y., Costa, K. D. & Covell, J. W. (2002) *Am J Physiol Heart Circ Physiol* **282,** H1510-1520.

16. Ashikaga, H., Omens, J. H. & Covell, J. W. (2004) *Am J Physiol Heart Circ Physiol* **287,** H1994-2002.

17. Waldman, L. K., Fung, Y. C. & Covell, J. W. (1985) *Circ Res* **57,** 152-63.

18. Ashikaga, H., Criscione, J. C., Omens, J. H., Covell, J. W. & Ingels, N. B., Jr. (2004) *Am J Physiol Heart Circ Physiol* **286,** H640-647.

19. Streeter, D. D., Jr., Spotnitz, H. M., Patel, D. P., Ross, J., Jr. & Sonnenblick, E. H. (1969) *Circ Res* **24,** 339-347.

20. Kindberg, K., Karlsson, M., Ingels, J., N. B. & Criscione, J. C. (2007) *Journal of Biomechanical Engineering* **129,** 603-610.

21. Hooks, D. A., Trew, M. L., Caldwell, B. J., Sands, G. B., LeGrice, I. J. & Smaill, B. H. (2007) *Circ Res* **101,** e103-112.

22. Harrington, K. B., Rodriguez, F., Cheng, A., Langer, F., Ashikaga, H., Daughters, G. T., Criscione, J. C., Ingels, N. B. & Miller, D. C. (2005) *Am J Physiol Heart Circ Physiol* **288,** H1324-1330.

23. Helm, P. A., Younes, L., Beg, M. F., Ennis, D. B., Leclercq, C., Faris, O. P., McVeigh, E., Kass, D., Miller, M. I. & Winslow, R. L. (2006) *Circ Res* **98,** 125-32.

24. Chen, J., Liu, W., Zhang, H., Lacy, L., Yang, X., Song, S.-K., Wickline, S. A. & Yu, X. (2005) *Am J Physiol Heart Circ Physiol* **289,** H1898-1907.

25. Chen, J., Song, S.-K., Liu, W., McLean, M., Allen, J. S., Tan, J., Wickline, S. A. & Yu, X. (2003) *Am J Physiol Heart Circ Physiol* **285,** H946-954.

26. William J. Karlon, J. W. C., Andrew D. McCulloch, John J. Hunter, Jeffrey H. Omens, (1998) *The Anatomical Record* **252,** 612-625.

27. Omens, J. H., Usyk, T. P., Li, Z. & McCulloch, A. D. (2002) *Am J Physiol Heart Circ Physiol* **282,** H680-687.

28. Zimmerman, S. D., Criscione, J. & Covell, J. W. (2004) *Am J Physiol Heart Circ Physiol* **287,** H2697-2704.

29. Dou, J., Reese, T. G., Tseng, W. I. & Wedeen, V. J. (2002) *Magnetic Resonance in Medicine* **48,** 105-114.

30. Sengupta, P. P., Khandheria, B. K., Korinek, J., Wang, J. & Belohlavek, M. (2005) *J Appl Physiol* **99,** 1104-11.